CrystEngComm

Accepted Manuscript

ROYAL SOCIETY OF CHEMISTRY

www.rsc.org/crystengcomm

Journal Name

RSCPublishing

ARTICLE

$La_2Ti_2O_7$ nanoplates decorated with Cu_2ZnSnS_4 nanoparticles for enhanced visible-light-driven photocatalytic activity

Cite this: DOI: 10.1039/x0xx00000x

Received 00th May 2014,
Accepted 00th May 2014

DOI: 10.1039/x0xx00000x

www.rsc.org/

Xiaomeng Tian,[a] Jingbing Liu, *[a] Hao Wang[a] and Hui Yan[a]

ABSTRACT: New visible-light-sensitive Cu_2ZnSnS_4 (CZTS) /$La_2Ti_2O_7$ hetero-junction photocatalysts have been successfully prepared via hydrothermal method and in-situ growth process. The catalyst was characterized by X-ray powder diffraction (XRD), scanning electron microscope (SEM), transmission electron microscope (TEM), and ultraviolet–visible–near-infrared (UV–vis–NIR) spectrophotometer. CZTS/ $La_2Ti_2O_7$ exhibited higher photocatalytic activity than pure $La_2Ti_2O_7$ and CZTS for the degradation of RhB under UV and visible light irradiation. The highest efficiency is observed with CZTS/ $La_2Ti_2O_7$ = 0.5. The enhancement of the photocatalytic activity of the CZTS/ $La_2Ti_2O_7$ hetero-junction photocatalyst could be ascribed to its improved light absorption property, high adsorption capacity and reduced recombination of the photoexcited electrons and holes during the photocatalytic reaction.

Introduction

Photocatalysis is considered to be a potential route for environmentally removing hazardous organic compounds with high energy efficiency.[1] As visible light accounts for the largest proportion of the solar spectrum, while the number of photocatalysts working under visible light irradiation is still limited,[2] so great efforts have been made to develop efficient visible light active photocatalysts.[3-6]

In recent years, composite photocatalysts with two or more components have been extensively explored, because it is difficult for a single photocatalyst to absorb visible light efficiently.[7-18] In addition, composite semiconductors can significantly reduce the recombination and speed up the separation rate of photogenerated charge carriers. Among various composite materials, the p–n hetero-junction structure has been demonstrated as an efficient method for separating electron and hole pairs,[19-30] such as Cu_2ZnSnS_4/WO_3,[31] Cu_2ZnSnS_4 /SnO_2[32], AgBr/WO_3,[33] AgX/Ag_3PO_4 (X = Cl, Br, I),[34] AgBr/H_2WO_4,[35] SnO_2/ZnO,[36] BiOI/TiO_2,[37] Bi_2O_3/Bi_2WO_6.[38]

N-type lanthanide titanate ($La_2Ti_2O_7$), as one of the layered compounds, has attracted widespread attention in the field of photocatalysis due to its unique layered structure, chemical activity and the peculiar electronic structure.[39-41] However, $La_2Ti_2O_7$ with large band gap can only exhibit high photocatalytic activity under ultraviolet (UV) light. This suggests that poor solar efficiency hinders its extensive application. Quaternary Cu_2ZnSnS_4 (CZTS), a direct-transition-type semiconductor possessing a narrow band gap energy of ca.1.5 eV and a large absorption coefficient (>$10^4 cm^{-1}$), has been recently found to be an excellent light energy-harvesting candidate for solar cells and photocatalysts.[42-44] In addition, CZTS consisting solely of nontoxic and inexpensive elements exhibits p-type semiconductor behavior.

Considering that CZTS and $La_2Ti_2O_7$ can be constructed to hetero-junction interface because of their matched band potentials, we report the design and fabrication of CZTS/ $La_2Ti_2O_7$ hetero-junction photocatalysts by hydrothermal method and in-situ growth process. The photocatalytic properties of CZTS/$La_2Ti_2O_7$ composites were investigated under both UV and visible light irradiation. Importantly, the novel CZTS/$La_2Ti_2O_7$ hetero-junction photocatalysts show broad and enhanced optical absorption from the ultraviolet to the visible light region. The photocatalytic mechanism based on the relative band positions of two semiconductors is proposed as well.

Experimental details

Sample preparation

All chemicals were of analytical grade and used without further purification. The $La_2Ti_2O_7$ powders were prepared by hydrothermal method. In a representative procedure, the equivalent molar quantities (5 mmol) of $La(NO_3)_3 \cdot 6H_2O$ and $Ti(SO_4)_2$ were dissolved in deionized water. Then aqueous solution containing 2.0 g NaOH was dropped into the above solution and meanwhile white precipitation appeared. The mixture was stirred for 10 min and then transferred into a

Teflon-lined stainless steel autoclave with a capacity of 50 mL, maintained at 200℃for 24 h, and subsequently cooled to room temperature. The white products were collected after filtration, washed with distilled water and ethanol several times and dried at 80℃.

The nanocomposite photocatalyst with CZTS were prepared by in-situ synthetic process. 1 mmol of pre-prepared $La_2Ti_2O_7$ was dispersed into ethylene glycol, and then the precursor of CZTS was prepared by the following method. 1mmol $CuCl_2$、0.5mmol $ZnCl_2$、0.5mmol $SnCl_2$、0.8mmol thioacetamide (the CZTS/ $La_2Ti_2O_7$ molar ratio is thus 0.5:1) was added in turn with magnetic stirring. The mixture was exposed to ultrasound irradiation in the air for another 30 mins and transferred into a 50 mL Teflon-lined stainless steel autoclave. The autoclave was heated at 180℃ for 15 h, and then cooled to room temperature naturally. After reaction, the resulting powders were repeatedly washed by centrifugation and decantation with deionized water, and then dried at 80℃ for 6 h. In the next procedure, the CZTS/ $La_2Ti_2O_7$ molar ratio was altered to 0.2:1 and 0.8:1 by changing the dosage of $CuCl_2$、$ZnCl_2$、$SnCl_2$ and thioacetamide. In addition, pure Cu_2ZnSnS_4 was prepared under the same condition for comparison.

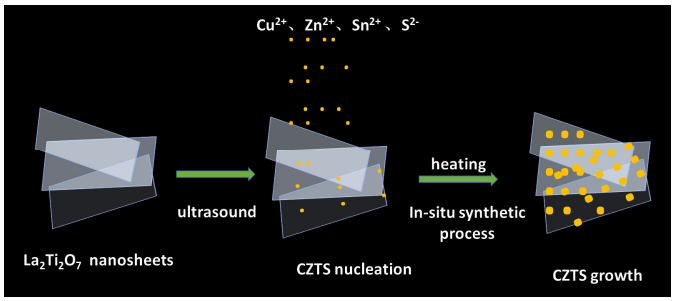

Fig. 1.The schematic diagram for the formation process of the nanocomposites.

Characterization

X-ray powder diffraction (XRD) patterns of the samples were recorded on a BRUKER D8 ADVANCE X-ray powder diffractometer with Cu Kα radiation (λ = 1.5406 Å). The accelerating voltage, emission current, and scanning speed were 40 kV, 40 mA and 0.2°/s, respectively. The morphologies and microstructures of the samples were observed using a Hitachi S4800 field emission scanning electron microscope (FESEM) and Hitachi-H8100 transmission electron microscope (TEM) with an accelerating voltage of 200 kV. Optical absorption studies were carried out using an ultraviolet-visible-near-infrared (UV–vis–NIR) spectrophotometer (Shimadzu UV-3101PC) using pure $BaSO_4$ pellet as the reference.

Photocatalytic Activity Tests

The photocatalytic performance tests were carried out by adding 50 mg of photocatalysts into 100 mL of 1.7×10^{-5} mol/L Rhodamine B (RhB) solution. The suspension was magnetically stirred in dark to establish adsorption/desorption equilibrium. Then the suspensions were irradiated under both ultraviolet light by using a 400 W high-pressure Hg lamp (λ < 280 nm) or visible light by a 500-W tungsten halogen lamp (λ> 400 nm), and then 5 mL of solution was taken out every 10 min and centrifuged to remove the photocatalyst powders. The concentration of RhB solution was determined by measuring the absorbance at 554 nm with the UV–vis spectrophotometer.

Results and discussion

Powder characterization by XRD and SEM

The XRD patterns of CZTS/ $La_2Ti_2O_7$ composites are shown in Fig. 2. The diffraction patterns of CZTS and $La_2Ti_2O_7$ are also presented for comparison. In the samples (Fig. 2a–d), the characteristic diffraction peaks at 2θ of 29.8°, 32.2°, and 40.0° are attributed to $La_2Ti_2O_7$ with a perovskite structure conforming to the P21 space group (JCPDS 70-0903). Meanwhile, there are several additional diffraction peaks at 2 θ of 28.6°, 47.5°, and 56.3°, which can be attributed to (112)、(220) and (312) crystal planes of the tetragonal CZTS phase (JCPDS 26-0575). From Fig. 2b–e, the peaks represented the CZTS are becoming stronger and stronger, indicating that the content of CZTS is increasing. The other diffraction peaks of CZTS in the nanocomposites can not be clearly identified because they overlap with the peaks of $La_2Ti_2O_7$. Moreover, in the nanocomposite samples, only the diffraction peaks of CZTS and $La_2Ti_2O_7$ are found, indicating that no other phase appears in the experimental procedure.

The morphologies of the products were characterized by SEM and TEM (Fig. 3). From Fig. 3a, it can be seen that the $La_2Ti_2O_7$ plates are very thin, with thickness of about 10 nm, which is in accordance with our previous results.[45] In Fig. 3b, the morphology of CZTS is irregular spherical particles of about 50 nm. As displayed in Fig. 3c-e, some CZTS nanoparticles homogenously disperse on the surfaces of the $La_2Ti_2O_7$ nanosheets, and the size of CZTS decreases to 30 nm or so. With the increasing CZTS content, more CZTS nanoparticles were dispersed on the surface of $La_2Ti_2O_7$, which formed the hetero-junction structure. But in Fig. 3e, the CZTS nanoparticles are so much that they cover the surface of $La_2Ti_2O_7$ nanosheets. To further obtain information about the structure of the sample, the CZTS/ $La_2Ti_2O_7$ with ratio of 0.5 was characterized by TEM. As shown in Fig. 3f, CZTS nanoparticles are tightly coupled on the surface of $La_2Ti_2O_7$ even when they are subjected to an ultrasonic treatment. High-resolution TEM images of the CZTS/ $La_2Ti_2O_7$ are shown in Fig. 2g, the clear lattice fringe indicates the co-existing of CZTS and $La_2Ti_2O_7$, in which the 0.313 nm of lattice spacing is closed to the (112) lattice planes of tetragonal CZTS, while the 0.310 nm of lattice spacing is corresponding to (220) lattice plane of perovskite structured $La_2Ti_2O_7$.

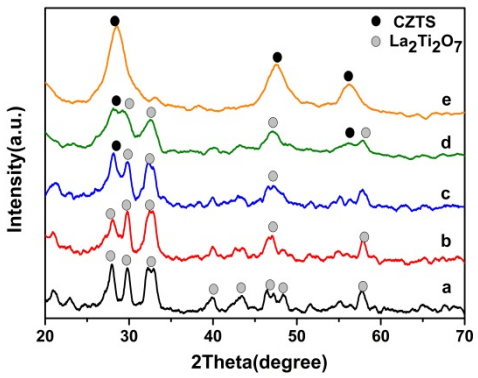

Fig.2 XRD patterns of $La_2Ti_2O_7$, CZTS, and CZTS / $La_2Ti_2O_7$ nanocomposites: (a) $La_2Ti_2O_7$; (b) CZTS / $La_2Ti_2O_7$ = 0.2; (c) CZTS / $La_2Ti_2O_7$ = 0.5; (d) CZTS / $La_2Ti_2O_7$ = 0.8; (e) CZTS.

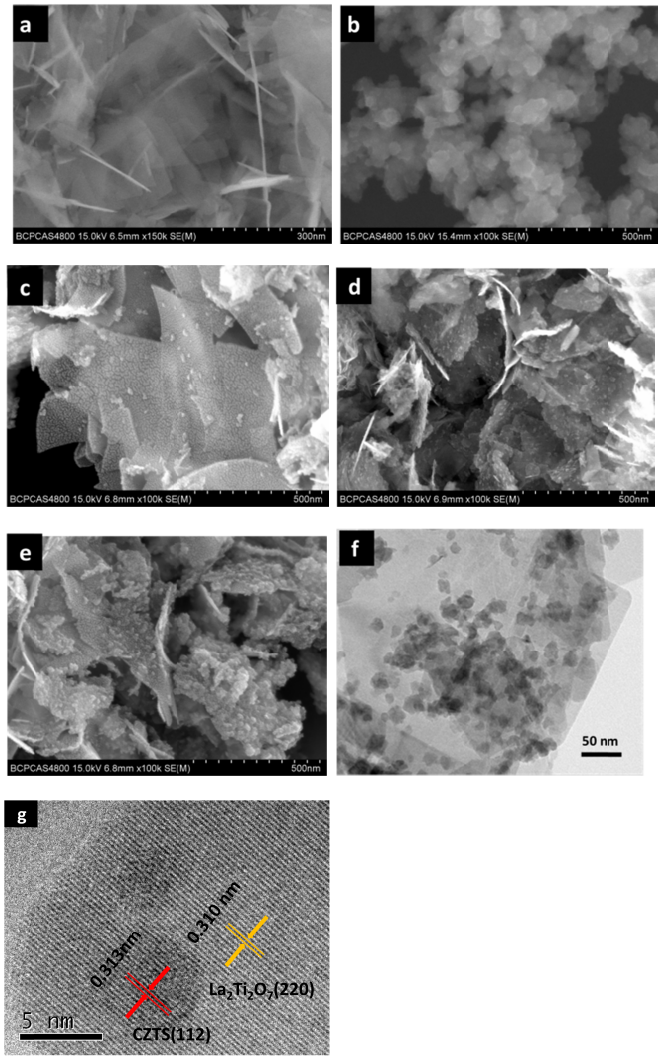

Fig. 3 SEM images of (a) $La_2Ti_2O_7$; (b) CZTS; and CZTS / $La_2Ti_2O_7$ nanocomposites, (c) CZTS / $La_2Ti_2O_7$ = 0.2; (d) CZTS / $La_2Ti_2O_7$ = 0.5; (e) CZTS / $La_2Ti_2O_7$ = 0.8; (f) and (g) TEM and HRTEM image of CZTS / $La_2Ti_2O_7$ nanocomposites with CZTS / $La_2Ti_2O_7$ = 0.5.

Photoabsorption properties

Fig. 4 shows the diffuse reflection spectra of the prepared samples. The band-gap of the products can be estimated from the onset of the absorption edge. For a crystalline semiconductor, the optical absorption near the band edge follows the equation $\alpha h\nu = A(h\nu - Eg)^{1/2}$, where α, ν , E_g , and A are absorption coefficient, light frequency, band gap, and a constant, respectively.[46]

The band gap of the $La_2Ti_2O_7$ nanosheets can be estimated to be 3.4 eV from the onset of the absorption edge, which only absorbs ultraviolet light due to the wide band gap. However, the CZTS/ $La_2Ti_2O_7$ nanocomposites show absorption in the visible-light region. We also observed that increasing CZTS concentration produces an increase of the junction absorptions. With the ratio of CZTS / $La_2Ti_2O_7$ increasing from 0.2 to 0.5, the energy gap decreases from approximately 2.7 eV to 2.5 eV , which are much higher than pure CZTS (1.5 eV). The results obtained signify that the hetero-junction can be excited by visible light.

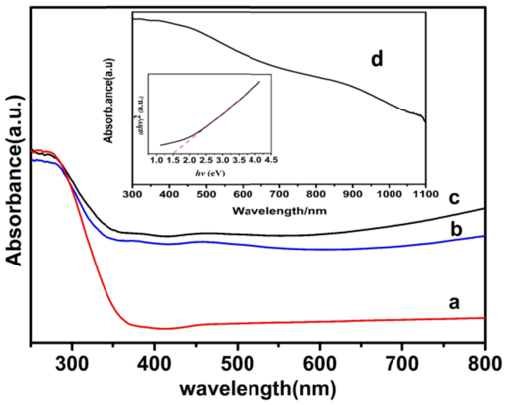

Fig. 4 UV–vis absorption spectra of (a) $La_2Ti_2O_7$; (b) CZTS / $La_2Ti_2O_7$ = 0.2; (c) CZTS / $La_2Ti_2O_7$ = 0.5;(d) CZTS

Evaluation of RhB removal efficiency by the CZTS/ $La_2Ti_2O_7$ nanocomposites

The photocatalytic activity of CZTS/ $La_2Ti_2O_7$ was probed by photodegradation of RhB. Firstly, the photocatalytic activity of the samples are tested under UV light irradiation, the results are shown in Fig. 5.

An interesting observation is that CZTS/ $La_2Ti_2O_7$ and CZTS exhibit much larger adsorption capacity for RhB than pure $La_2Ti_2O_7$. Many researches indicate that the enhancement of adsorption was ascribed to the increase of surface acidity after composing with semiconductor photocatalyst.[47, 48] Therefore, the increase of adsorption capacity may be ascribed to the CZTS that facilitates the formation of increased amount of adsorption sites on $La_2Ti_2O_7$ surface. Furthermore, the highly dispersed CZTS nanoparticles on the surface of $La_2Ti_2O_7$ sheets are much smaller than pure CZTS nanoparticles and thus have larger surface area accessible to RhB molecules. In summary, this strong adsorption capacity of CZTS/ $La_2Ti_2O_7$ nanocomposites and CZTS could be attributed to its surface states and larger specific surface area.

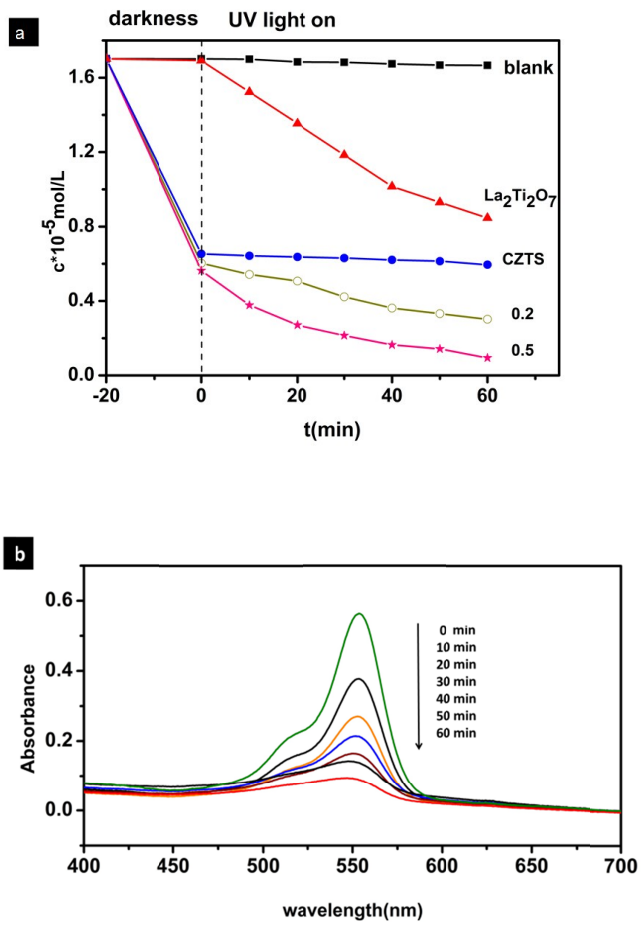

Fig. 5a The concentration of RhB as a function of irradiation time under ultraviolet light; b Degradation curves of RhB irritated under ultraviolet light with CZTS / $La_2Ti_2O_7$ = 0.5

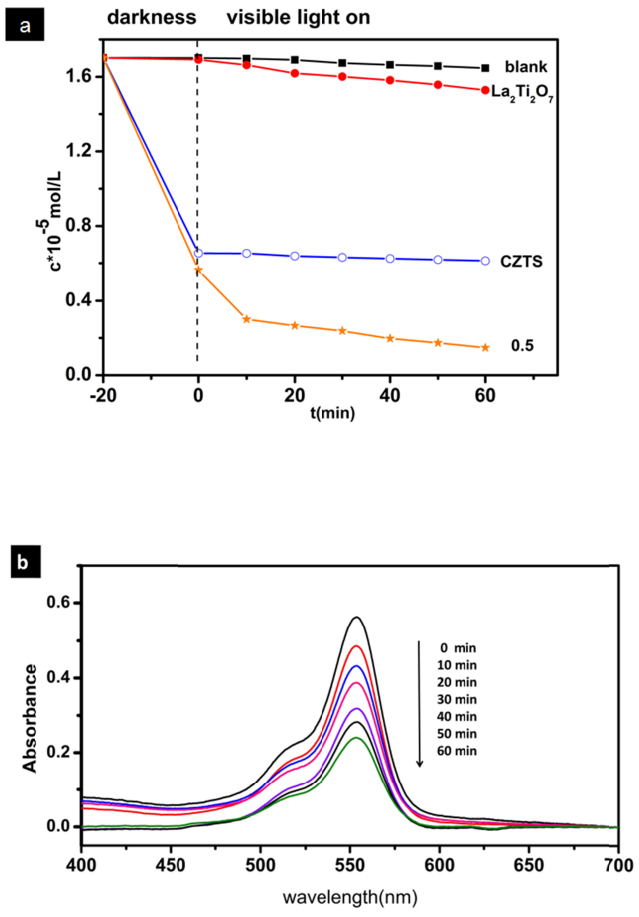

Fig. 6a The concentration of RhB as a function of irradiation time under visible light; b Degradation curves of RhB irritated under visible light with CZTS / $La_2Ti_2O_7$ = 0.5

From Fig. 5a, it can be observed that almost no RhB was degraded in the absence of samples under UV light. The curve of pure CZTS demonstrates that almost no RhB degradation occurs after the adsorption equilibrium, while pure $La_2Ti_2O_7$ exhibits photocatalytic activity. Furthermore, CZTS/ $La_2Ti_2O_7$ nanocomposites show an even higher photocatalytic activity, and meanwhile, the degradation rate by nanocomposite with the ratio of CZTS/ $La_2Ti_2O_7$ =0.5 reaches nearly 95% after 60 min.

Fig. 5b depicts the temporal evolution of the spectra during the photodegradation of RhB mediated by the CZTS/ $La_2Ti_2O_7$ nanocomposites. The intensity of the adsorption peaks diminishes gradually as the exposure time increases under UV light irradiation, which indicates that the RhB were removed during irradiation.

The photocatalytic activity of the samples was also evaluated with a 500-W tungsten halogen lamp ($\lambda > 400$ nm), which can provide visible light irradiation. From Fig. 6a, it can be seen that only a slight decrease in the concentration of RhB is detected by $La_2Ti_2O_7$, because pure $La_2Ti_2O_7$ with wide band gap cannot response to visible light well. However, the CZTS/ $La_2Ti_2O_7$ nanocomposites exhibit high photocatalytic activity under visible light irradiation. The result demonstrates that the hetero-junction structure of CZTS/ $La_2Ti_2O_7$ can improve the photocatalytic activity to degrade RhB under visible light irradiation.

The time-dependent degradation curves of RhB are also made in Fig. 6b, in order to make sure that RhB diminishes gradually as the exposure time increases under visible light irradiation.
In CZTS/ $La_2Ti_2O_7$ system, $La_2Ti_2O_7$ is an n-type semiconductor and CZTS is a p-type semiconductor. When they were combined, a p–n-type hetero-junction would be produced. It was also reported that at the thermodynamic equilibrium of a p–n hetero-junction, there was an internal field with direction from n-type to p-type, which is conducive to the separation of electrons and holes. The migration direction of the photogenerated charge carrier depends on the band edge positions of the two semiconductors. We could determine the

flat band potential of the photocatalysts approximately according to Eqs. (1):[49]

$$V_{fb}(NHE)=2.94-E_g \quad (1)$$

Where V_{fb} and E_g represent a flat band potential and a band gap, respectively. This equation could be applied for oxide semiconductor photocatalysts consisting of a metal cation with a d0 or d10 configuration. According to Eqs. (1), the bottom of the conduction band level and the top of the valence band potential of $La_2Ti_2O_7$ nanosheets were estimated to be -0.46 and +2.94 eV (vs NHE), respectively. It has also been reported that the position of the conduction band minimum and valence band maximum of CZTS are -1.3 and 0.2 eV respectively.[50] These thermodynamic conditions favor the phenomenon of electron injections. And the most plausible mechanism for the degradation of pollutants under visible light irradiation is also proposed in Fig.7.

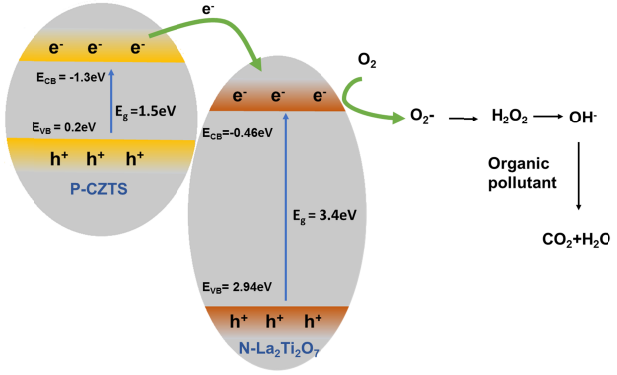

Fig. 7. Proposed mechanism for the visible light photodegradation of RhB on hetero-junction photocatalysts CZTS/ $La_2Ti_2O_7$

Under visible light irradiation, electrons (e) in the valence band (VB) of CZTS were excited to conduction band (CB), leaving behind electron holes on its valence band. As we know that the internal field plays a very important role in the CZTS/ $La_2Ti_2O_7$ hetero-junction structure, so electrons in the conduction band of CZTS were easily injected into the CB of $La_2Ti_2O_7$ because the CB of CZTS is more negative than that of $La_2Ti_2O_7$. And then the electrons and holes generated in CZTS are separated. These electrons react at the surface with dissolved oxygen molecules and induce a formation of oxygen peroxide radicals O^{2-} and H_2O_2, and then to hydroxyl radicals.[51] These hydroxyl radicals can activate some unsaturated organic pollutants, leading to their subsequent decomposition. Then the photocatalytic reaction can be enhanced greatly.

In addition, the large adsorption capacity may also contribute to the enhanced photocatalytic performance, CZTS/ $La_2Ti_2O_7$ can largely and rapidly enrich RhB molecules onto its surface, and then the adsorbed RhB can be effectively removed by photocatalytic degradation.

Conclusions

In summary, the hetero-junction photocatalysts CZTS/ $La_2Ti_2O_7$ have been designed and prepared via hydrothermal method and in-situ growth process. It has an optimal activity at the CZTS/$La_2Ti_2O_7$=0.5 catalyst and exhibited much higher photocatalytic activity than pure $La_2Ti_2O_7$ and CZTS for the degradation of RhB under UV and visible light irradiation. The remarkable enhancement of the photocatalytic performance under visible light is ascribed mainly to the adopting of CZTS, which is a visible light absorbing semiconductor with a relatively narrow band gap. The CZTS/ $La_2Ti_2O_7$ hetero-junction also improved the prevention of the recombination of photogenerated electron–hole pairs. In addition, the high adsorption capacity facilitated surface accessibility, resulting in the high photocatalytic activity. The CZTS/ $La_2Ti_2O_7$ hetero-junction photocatalysts should find wide applications in environmental pollution control, solar energy conversion, and other related areas.

Acknowledgements

This work was supported by the Foundation on the Creative Research Team Construction Promotion Project of Beijing Municipal Institutions, 2013 Annual Rixin Training Support Project of Beijing University of Technology, and Natural Science Foundation of Beijing (No. 2112008)

Notes and references

[a] The College of Materials Science and Engineering, Beijing University of Technology, Beijing 100124, PR China. Fax: 86-10-67392733; Tel: 86-10-67392733; E-mail:liujingbing@bjut.edu.cn.

References:

1. G. Palmisano, V. Augugliaro, M. Pagliaro and L. Palmisano, *Chem Commun*, 2007, 3425-3437.
2. B. Zhang, J. K. Jian, Y. Zheng, Y. Sun, Y. Chen and L. Cui, *Mater Lett*, 2008, **62**, 1827-1830.
3. Z. Liu, Z. Zhao and M. Miyauchi, *The Journal of Physical Chemistry C*, 2009, **113**, 17132-17137.
4. H. Wang, S. Li, L. Zhang, Z. Chen, J. Hu, R. Zou, K. Xu, G. Song, H. Zhao and J. Yang, *CrystEngComm*, 2013, **15**, 9011-9019.
5. W. Yang, Y. Liu, Y. Hu, M. Zhou and H. Qian, *J Mater Chem*, 2012, **22**, 13895-13898.
6. X. Liu, J. Hu, J. Li, Y. Hu, Y. Shao, H. Yang, G. Tong and H. Qian, *Mater Lett*, 2013, **91**, 129-132.
7. T. Li, L. Zhao, Y. He, J. Cai, M. Luo and J. Lin, *Applied catalysis. B, Environmental*, 2013, **129**, 255-263.
8. Y. C. Zhang, J. Li and H. Y. Xu, *Applied Catalysis B: Environmental*, 2012, **123**, 18-26.
9. N. Wetchakun, S. Chaiwichain, B. Inceesungvorn, K. Pingmuang, S. Phanichphant, A. I. Minett and J. Chen, *ACS applied materials & interfaces*, 2012, **4**, 3718-3723.
10. W. Li, D. Li, S. Meng, W. Chen, X. Fu and Y. Shao, *Environ Sci Technol*, 2011, **45**, 2987-2993.
11. Z. Zhang, W. Wang, L. Wang and S. Sun, *ACS applied materials & interfaces*, 2012, **4**, 593-597.

12. Y. Shi, H. Li, L. Wang, W. Shen and H. Chen, *ACS applied materials & interfaces*, 2012, **4**, 4800-4806.
13. M. Pelaez, N. T. Nolan, S. C. Pillai, M. K. Seery, P. Falaras, A. G. Kontos, P. S. Dunlop, J. W. Hamilton, J. A. Byrne and K. O'Shea, *Applied Catalysis B: Environmental*, 2012, **125**, 331-349.
14. Y. He, J. Cai, T. Li, Y. Wu, H. Lin, L. Zhao and M. Luo, *Chem Eng J*, 2013, **215**, 721-730.
15. Y. Feng, N. Feng, G. Zhang and G. Du, *CrystEngComm*, 2014, **16**, 214-222.
16. L. Chen, D. Jiang, T. He, Z. Wu and M. Chen, *CrystEngComm*, 2013, **15**, 7556-7563.
17. P. Hu, X. Hu, C. Chen, D. Hou and Y. Huang, *CrystEngComm*, 2013, **16**, 649-653.
18. Y. Lin, F. Zhang, D. Pan, H. Li and Y. Lu, *J Mater Chem*, 2012, **22**, 8759-8763.
19. H. Xu, H. Li, C. Wu, J. Chu, Y. Yan, H. Shu and Z. Gu, *J Hazard Mater*, 2008, **153**, 877-884.
20. S. C. Yan, S. B. Lv, Z. S. Li and Z. G. Zou, *Dalton Transactions*, 2010, **39**, 1488-1491.
21. M. Guan, D. Ma, S. Hu, Y. Chen and S. Huang, *Inorg Chem*, 2010, **50**, 800-805.
22. Y. Yuan, S. Cao, Y. Liao, L. Yin and C. Xue, *Applied Catalysis B: Environmental*, 2013, **140**, 164-168.
23. V. Etacheri, G. Michlits, M. K. Seery, S. J. Hinder and S. C. Pillai, *ACS applied materials & interfaces*, 2013, **5**, 1663-1672.
24. Y. Lin and Y. Hsu, *Applied Catalysis B: Environmental*, 2013, **130**, 93-98.
25. F. Xiao, *ACS applied materials & interfaces*, 2012, **4**, 7055-7063.
26. T. J. Athauda, J. G. Neff, L. Sutherlin, U. Butt and R. R. Ozer, *ACS applied materials & interfaces*, 2012, **4**, 6917-6926.
27. D. He, L. Wang, D. Xu, J. Zhai, D. Wang and T. Xie, *ACS applied materials & interfaces*, 2011, **3**, 3167-3171.
28. J. Cao, B. Xu, H. Lin and S. Chen, *Chem Eng J*, 2013, **228**, 482-488.
29. M. Gui, W. Zhang, Y. Chang and Y. Yu, *Chem Eng J*, 2012, **197**, 283-288.
30. A. Nashim and K. M. Parida, *Chem Eng J*, 2013, **215**, 608-615.
31. M. Miyauchi, T. Hanayama, D. Atarashi and E. Sakai, *The Journal of Physical Chemistry C*, 2012, **116**, 23945-23950.
32. X. Lin, B. Huang, Z. Wang, W. Wang, Y. Dai, X. Zhang and X. Qin, *Mater Lett*, 2013, **99**, 146-149.
33. J. Cao, B. Luo, H. Lin and S. Chen, *J Hazard Mater*, 2011, **190**, 700-706.
34. Y. Bi, S. Ouyang, J. Cao and J. Ye, *Phys Chem Chem Phys*, 2011, **13**, 10071-10075.
35. J. Cao, B. Luo, H. Lin and S. Chen, *Journal of Molecular Catalysis A: Chemical*, 2011, **344**, 138-144.
36. L. Zheng, Y. Zheng, C. Chen, Y. Zhan, X. Lin, Q. Zheng, K. Wei and J. Zhu, *Inorg Chem*, 2009, **48**, 1819-1825.
37. X. Zhang, L. Zhang, T. Xie and D. Wang, *The Journal of Physical Chemistry C*, 2009, **113**, 7371-7378.
38. M. Gui, W. Zhang, Q. Su and C. Chen, *J Solid State Chem*, 2011, **184**, 1977-1982.
39. D. Arney, B. Porter, B. Greve and P. A. Maggard, *Journal of Photochemistry and Photobiology A: Chemistry*, 2008, **199**, 230-235.
40. D. W. Hwang, H. G. Kim, J. S. Lee, J. Kim, W. Li and S. H. Oh, *The Journal of Physical Chemistry B*, 2004, **109**, 2093-2102.
41. W. Shangguan and A. Yoshida, *The Journal of Physical Chemistry B*, 2002, **106**, 12227-12230.
42. K. Jimbo, R. Kimura, T. Kamimura, S. Yamada, W. S. Maw, H. Araki, K. Oishi and H. Katagiri, *Thin Solid Films*, 2007, **515**, 5997-5999.
43. H. Katagiri, *Thin Solid Films*, 2005, **480**, 426-432.
44. H. Katagiri, K. Saitoh, T. Washio, H. Shinohara, T. Kurumadani and S. Miyajima, *Sol Energ Mat Sol C*, 2001, **65**, 141-148.
45. K. Li, Y. Wang, H. Wang, M. Zhu and H. Yan, *Nanotechnology*, 2006, **17**, 4863.
46. X. Zhang, Z. Ai, F. Jia and L. Zhang, *The Journal of Physical Chemistry C*, 2008, **112**, 747-753.
47. F. Chen, Z. Liu, Y. Liu, P. Fang and Y. Dai, *Chem Eng J*, 2013, **221**, 283-291.
48. M. A. Abdullah and F. K. Chong, *Chem Eng J*, 2010, **158**, 418-425.
49. J. Zeng, H. Wang, Y. Zhang, M. K. Zhu and H. Yan, *The Journal of Physical Chemistry C*, 2007, **111**, 11879-11887.
50. T. Arai, S. Tajima, S. Sato, K. Uemura, T. Morikawa and T. Kajino, *Chem Commun*, 2011, **47**, 12664.
51. S. Sakthivel and H. Kisch, *Angewandte Chemie International Edition*, 2003, **42**, 4908-4911.

